Supplementary Material to the article "Semiclassical scattering by edge imperfections in topological insulators under magnetic field"

A Semiclassical equation

A.1 Derivation of the main semiclassical exponential and pre-exponential term

We plug in (9) into the main differential equation (6) and perform the formal expansion in powers of $\hbar$. Neglecting the terms of order $\hbar$ (the zeroth order semiclassical expansion) results in the following quadratic equation on $S_0'(x)$:

$$4(\varepsilon+\mu)[(1+\varphi^2)(S_0')^2+2\mu\varphi S_0'] = 4(\varepsilon+\mu)(\varepsilon^2-\mu^2) \tag{S1}$$

which solution is written in the main text (11). Next, keeping the next terms (of the order of $\hbar$) we get a linear equation on $S_1(x)$:

$$S_{1,\pm} = i\int\left(\mp\frac{\varepsilon}{2p}+\frac{\varphi\varepsilon^2}{p^2}+\frac{\mu q_\pm}{2p^2}\right)d\varphi, \tag{S2}$$

where p is defined in Eq. 11. The integration gives $S_1(x) = -i\ln(\xi_1)$, ξ_1 is written in the main text (12).

A.2 Validity of semiclassical expansion near the branch point of p.

The validity of the semiclassical approach is checked as follows [1]. We need to make sure that the 1st order correction (in $\hbar$) to the l.h.s. of (S1) is much smaller then the zeroth order expression.

The first order in $\hbar$ term then reads:

$$\begin{aligned}\text{l.h.s. of (S1)}\Big|_{1^{\text{st}}\text{ order in }\hbar} &= -4i(\varepsilon+\mu)\hbar\varphi' \\ \times\frac{p[\varepsilon(\varphi^2+1)-\mu]+2\varepsilon^2\varphi(\varphi^2+1)-\mu^2\varphi}{p(\varphi^2+1)}&\end{aligned} \tag{S3}$$

Now expand momentum p near the branch point $p=0$ using the expansion of the field φ: $\varphi(z) = i\sqrt{1-(\mu/\varepsilon)^2}+i\delta z/a$. We see from the start that, unlike the denominator, the nominator of (S3) does not vanish as $p\to 0$. That means the first order semiclassical correction diverges at the branch point $p=0$. Plugging in $p=0$ in the nominator of (S3) while keeping it finite in the denominator and setting $\varphi^2+1=(\mu/\varepsilon)^2$ we obtain the following (in the first order of $\hbar$):

$$\text{l.h.s. of (S1)} = 2^{3/2}\hbar(\varepsilon+\mu)(\varepsilon^2-\mu^2)^{1/4}\sqrt{\frac{\varepsilon}{a\delta z}} \tag{S4}$$

Dividing it by the r.h.s. of (S1) (and squaring it for the sake of beauty) we obtain condition discussed after Eq.(16) of applicability of the semiclassical expansion near the branch point of p in the main body of the paper.

A.3 The correspondence between Schrödinger and Dirac equation

The goal of this paragraph is to show the full equivalence of semiclassical solutions following from the Schrödinger equation (18) and the main Dirac equation (6). Expanding $\pi^2(x)$ formally in powers of $\hbar$ and keeping the first in $\hbar$ terms only we obtain:

$$\pi(x) = \frac{1}{\hbar}\frac{p}{\varphi^2+1}-\frac{i}{2p}\frac{\varepsilon-\mu+\varepsilon\varphi^2}{(\varphi^2+1)}\varphi'+... \tag{S5}$$

Next we write down the semiclassical solution in the standard way:

$$\theta_\pm(x) = \frac{1}{\sqrt{\pi(x)}}\exp\left(\pm i\int^x\pi(x)\,dx\right) \tag{S6}$$

Finally, we perform the integration and express the semiclassical action in two convenient ways:

$$\begin{aligned}\int^x\pi(x)\,dx &= -\frac{i}{2}\ln\frac{(p+\varphi\varepsilon)q_+\sqrt{\varphi^2+1}}{\varepsilon^2-\mu^2} \\ &\equiv -\frac{i}{2}\ln\frac{\varepsilon^2-\mu^2}{(p-\varphi\varepsilon)q_-\sqrt{\varphi^2+1}}\end{aligned} \tag{S7}$$

Now, we make the expansion of $\eta(x)$ function up to the first in $\hbar$ terms:

$$\frac{\eta(x)}{2} = \frac{i}{\hbar}\frac{\mu\varphi}{\varphi^2+1}+\frac{3}{2}\frac{\varphi\varphi'}{\varphi^2+1} \tag{S8}$$

and perform integration (in view of formula (19)):

$$\int^x\frac{\eta(x)\,dx}{2} = \frac{i}{\hbar}\int\frac{\mu\varphi\,dx}{\varphi^2+1}+\frac{3}{4}\ln(\varphi^2+1) \tag{S9}$$

Combining two variants of action (S7), the integral (S9) and solution (S6) and plugging the latter into wave function (19) we obtain the exact correspondance with semiclassical expressions (11)-(12).

A.4 The expansion of the Schroedinger equation near the branch point

In the vicinity of the branch point $z_\pm$ we have:

$$\eta(\zeta) = -\frac{2}{\hbar}\frac{\varepsilon\sqrt{\varepsilon^2-\mu^2}}{\mu}+... \tag{S10}$$

Now, the question is the expansion of $\pi^2(z)$ near $z_\pm$. It has the following form:

$$\pi^2(\zeta) = \underbrace{i\frac{(\varepsilon-\mu)\varepsilon^3}{\mu^3}\frac{1}{\hbar a}}_{\text{I}} + \underbrace{\frac{1}{\hbar^2}\frac{2i\zeta}{a}\frac{\epsilon^5\sqrt{\varepsilon^2-\mu^2}}{\mu^4}}_{\text{II}} + \ldots \quad \text{(S11)}$$

Interestingly, once we take into account z dependence of the potential $\varphi(z)$ the potential stops vanishing at $z = z_\pm$. Let us prove that this is consistent with our analysis and this term can be discarded in comparison to the second one. We are interested in estimates, therefore we put $\varepsilon \sim \mu$ everywhere in our arguments. Suppose ζ is chosen in such a way that the first terms dominates over the second one:

$$\frac{\text{II}}{\text{I}} \sim \frac{z\varepsilon}{\hbar} \ll 1 \quad \text{(S12)}$$

Then we have for the solution of (18) in the main body:

$$\theta(\zeta) \sim \exp\left(\#\sqrt{\frac{\varepsilon}{\hbar a}}\zeta\right). \quad \text{(S13)}$$

From the exponent of the (S13) we conclude that the characteristic scale of the wave function is $\sqrt{\hbar a/\varepsilon}$.

$$\frac{\text{II}}{\text{I}} = \sqrt{\frac{a\varepsilon}{\hbar}} \gg 1 \text{ (see Eq. 8)} \quad \text{(S14)}$$

Therefore, in the region of interest (on the scale of a supposed semiclassical wave length) term I can be safely discarded comparing to II.

Let us check that retaining just term II in (S11) is consistent with the analysis. If only term II is retained, the solution of (18) in the semiclassical regime reads:

$$\theta(\zeta) \propto \exp\left(i\int^\zeta \pi(\zeta)d\zeta\right) \sim \exp\left(\#\frac{\zeta^{3/2}}{\sqrt{a}}\frac{\varepsilon}{\hbar}\right). \quad \text{(S15)}$$

As a result, the characteristic scale of the wave function is $(a\hbar^2/\varepsilon)^{1/3}$. Therefore, we have for the ratio:

$$\frac{\text{II}}{\text{I}} = \left(\frac{a\varepsilon}{\hbar}\right)^{1/3} \gg 1 \quad \text{(S16)}$$

And indeed, this coincides with our initial statement. This way, term I in (S11) can be safely discarded, which concludes the validity of the semiclassical equation (24) in the main body of the paper.

B Analytic properties of Airy function asymptotics

B.1 Semiclassical analysis of the Airy equation

We determine the position of the anti-Stokes lines using the semiclassical analysis of Eq. (24) in the main body at large values of ζ: $\theta(\zeta) \propto \exp[i\int^\zeta \pi(t)dt]$, $\int^\zeta \pi(t)dt \gg 1$:

$$\mathrm{Im}\int_0^s \pi(t)\,dt = 0 \Rightarrow \mathrm{Im}\, s^{3/2} = 0 \;\Rightarrow \arg s = \frac{2\pi n}{3}, \quad n \in \mathbb{Z} \quad \text{(S17)}$$

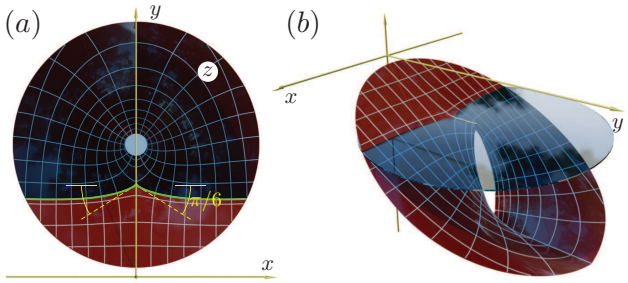

Figure S1: Exact anti-Stokes lines for the deformation profile $\varphi(z) = ze^{-z^2/2}$ presented as a cross-section of the integral $h(z) = \mathrm{Im}\int_0^z \pi(t)\,dt$ and the level plane $h = h(z_+)$. (a) The top view. The anti-Stokes line marked as a green line. The Stokes line is presented as a black dashed line. (b) Axonometric view. One clearly sees, how the anti-Stokes line becomes horizontal far from the turning point. The hole in the center is the circular vicinity of the singularity z_0 of $\pi(z)$, where $\varphi(z_0) = i$.

As we see from (S17), the anti-Stokes lines are separated by angle $2\pi/3$. The pattern of anti-Stokes lines for the typical profile function $\varphi(z) = ze^{-z^2/2}$ is presented in Fig. S1, where the anti-Stokes lines are drawn as level lines of the surface of semiclassical action with exact momentum $\mathrm{Im}\int_0^\zeta \pi(t)dt$. The anti-Stokes lines in Fig. S1 are drawn for non-rescaled coordinate z.

As a result, the semiclassical wave functions (22) in the vicinity of $z_\pm$ on the anti-Stokes line $n = 0$ are given by Eq. 25 in the main body.

B.2 Exact solution and steepest descent analysis of the Airy equation

To solve (24) we use the Laplace method of solution of differential equations with linear coefficients [2]. We use a concise exposition and notation from [1]. To find the exact solution of the equation of the type:

$$\sum_{m=0}^{n}(a_m + b_m s)\frac{d^m\theta}{ds^m} = 0 \quad \text{(S18)}$$

we compose the polynomials:

$$P(t) = \sum_{m=0}^{n} a_m t^m, \quad Q(t) = \sum_{m=0}^{n} b_m t^m, \quad \text{(S19)}$$

And define the function:

$$Z(t) = \frac{1}{Q}\exp\int\frac{P}{Q}\,dt \quad \text{(S20)}$$

determined up to a multiplicative factor. Then the exact solution of (S18) can be found in terms of a contour integral:

$$\theta(s) = \int_C e^{st}Z(t)\,dt \quad \text{(S21)}$$

where contour C is chosen in such a way that function

$$V = e^{st}QZ \quad \text{(S22)}$$

assumes identical values at its ends. The V function controls the placement of the integration contour C in the exact solution (S21).

For the case of Airy equation:

$$\theta''(s) + s\theta(s) = 0 \tag{S23}$$

the P and Q polynomials:

$$P = t^2, \quad Q = 1 \;\Rightarrow\; Z(t) = e^{\frac{t^3}{3}} \tag{S24}$$

Combining (S24) and (S21) we obtain the integral representation

$$\theta(s) = \text{const} \int_C e^{st + \frac{t^3}{3}}\, dt \tag{S25}$$

coinciding up to normalization constant with (26). Function V is defined as:

$$V(t, s) = e^{st + \frac{t^3}{3}} \tag{S26}$$

Now we need to choose the contour. Usually, the easiest points where V assumes identical values to locate are the points where V vanishes. In case of a function as simple as (S26) it is enough to look at the large t behavior of the exponent: $st + t^3/3 \underset{t\to\infty}{\to} t^3/3$. We see, that at large t V vanishes as long as

$$\cos(3\arg t) < 0, \;\; |t| \to \infty \Rightarrow$$
$$\arg t \in \left(\frac{\pi}{6} + \frac{2\pi n}{3}, \;\; \frac{\pi}{2} + \frac{2\pi n}{3}\right) \tag{S27}$$

Equation S27 outlines the whole regions in the complex plane t where contour C should start and end. These regions are painted with gray color in Fig. 3 in the main part. They are also presented in Fig. S2 with intersecting horizontal plane and denoted I, II and III for $n = 1, 2$ and 3 in Eq. S27 respectively. It is important to note that regions (S27) are independent of the arguments of complex variable s.

B.3 Asymptotics at $s \to +\infty$

We need to place the contour in such a way that solution $\theta(s)$ has correct asymptotics at large positive value of s. That means, the integral (S25) should be computed with the steepest descent method. To this end, we need to know possible stationary points of the exponent function of solution (S25):

$$f(t) = st + \frac{t^3}{3} \tag{S28}$$

These are the saddle points:

$$t_1 = i\sqrt{s}, \quad t_2 = -i\sqrt{s} \tag{S29}$$

The second derivatives of function $f(t)$ at saddle points:

$$f''(t_1) = 2i\sqrt{s}, \quad f''(t_2) = -2i\sqrt{s} \tag{S30}$$

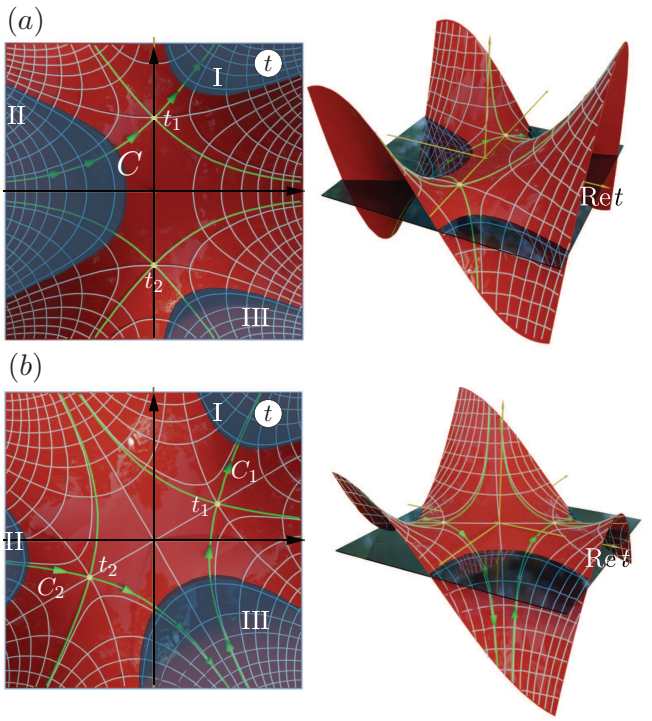

Figure S2: The relief of the real part of function $f(t) = st + t^3/3$ as a function of t. The grid is composed of the stationary lines of $f(t)$. The thin green contours are the steepest descent and ascent lines. They cross at two saddles (little yellow spheres). We also draw the horizontal plane for demonstrative purpose. The plane outlines the regions (I, II, III) where the value of $\mathrm{Re}\, f(t)$ tends to $-\infty$. These are the allowed regions for the end points of the placement of contour C (function $V(s) \to 0$ in these regions). These regions are also shown with gray color in Fig. 3. (a) corresponds to $\arg s = 0$, (b) corresponds to $\arg s = -2\pi/3$.

And the steepest descent directions at the saddles are given by the following relations:

$$\arg t = \frac{\pi}{2} - \frac{\arg f''}{2} + \pi n, \quad n \in \mathbb{Z} \;\Rightarrow \tag{S31}$$
$$\alpha_1 = \frac{\pi}{4} + \pi n, \quad \alpha = -\frac{\pi}{4} + \pi n \tag{S32}$$

The value of $f(t)$ at t_1 gives the main exponential value of solution (S25) in the saddle point approximation: $\theta \propto \exp(2is^{3/2}/3)$ which matches the outgoing wave semiclassical asymptotics θ_+^{app} from (25). Therefore, contour C in (S25) should be placed in such a way that it may be deformed into the steepest descent path going through saddle t_1. This placement is depicted in Fig. S2(a) and the saddle point approximation yields:

$$\theta(s) = \text{const}\sqrt{\frac{2\pi}{|f''(t_1)|}} e^{f(t_1) + i\alpha_1} = \text{const}\frac{\sqrt{\pi}}{s^{1/4}} e^{\frac{2i}{3}s^{3/2} + \frac{i\pi}{4}} \tag{S33}$$

Comparing asymptotics (S33) and semiclassical expression for θ_+^{app} in (25) we easily fixate the constant in front of the integral:

$$\text{const} = \frac{e^{-i\pi/4}}{\sqrt{\pi}\gamma^{1/6}}, \tag{S34}$$

arriving at normalized solution (26).

B.4 Asymptotics at $s \to \infty e^{-2\pi i/3}$

After we rotate the argument of s by $-2\pi/3$ to transfer to the respective anti-Stokes line the topography of the relief of $\mathrm{Re}\, f(t)$ changes. The relief $\mathrm{Re} f(t)$ and its steepest descent paths at $s = |s|\exp(-2\pi i/3)$ are presented in Fig. S2(b). As we see, it is now possible to deform the initial contour C in such a way that it still begins in region II and ends in region I, yet it is split into two steepest descent paths C_1 and C_2 each of which passes via the respective saddle. The steepest descent directions at saddles follow from condition (S31).

$$\alpha_1 = \frac{5\pi}{12}, \quad \alpha_1 = -\frac{\pi}{12} \tag{S35}$$

And the contribution from two saddles reads:

$$\theta(s) = \mathrm{const}\frac{\sqrt{\pi}}{|s|^{1/4}}\left(e^{\frac{2i}{3}s^{3/2}+\frac{5\pi i}{12}} + e^{-\frac{2i}{3}s^{3/2}-\frac{\pi i}{12}}\right) \tag{S36}$$

Asymptotics (S36) together with (S34) gives formula (27) in the main part of the paper.

C Exact equation

C.1 Transformation of the Dirac equation

Equation (6) in the vicinity of the turning point z_p: $\varphi(z) \approx ia/(z-z_p)$ and in the limit $|\zeta| = |z-z_p| \ll |a|$ becomes ($\hbar = 1$):

$$\begin{aligned} 4a\zeta\Big[&a\zeta\psi_1''\left(2\zeta^2[\mu+\varepsilon]-a\right) \\ &+\psi_1'\left(a^2+4\mu\zeta^4[\mu+\varepsilon]-2a\zeta^2[4\mu+3\varepsilon]\right)\Big] \\ &+\psi_1\Big[-3a^3+2a^2(7\mu+9\varepsilon)\zeta^2 \\ &+4a(\mu+\varepsilon)(3\varepsilon-5\mu)\zeta^4-8(\varepsilon-\mu)(\mu+\varepsilon)^2\zeta^6\Big] = 0 \end{aligned} \tag{S37}$$

Surprisingly, Eq. S37 can be solved in quadratures for $\mu \neq 0$ and in elementary functions for $\mu = 0$. Let us first study its asymptotics at $\zeta \to \infty$ and $\zeta \to 0$. Retaining only the highest powers of ζ at $\zeta \to \infty$ we obtain the following equation:

$$\begin{aligned} a^2\psi_1'' + 2\zeta\mu a\psi_1' - \zeta^2(\varepsilon^2-\mu^2)\psi_1 = 0 \quad &\Longrightarrow \\ \psi_1 = e^{\frac{\zeta^2}{2a}(\varepsilon\pm\mu)}, \quad &\zeta \to \infty \end{aligned} \tag{S38}$$

At $\zeta \to 0$ we retain the lowest powers of ζ to obtain:

$$4u^2\psi_1'' - 4\zeta\psi_1' + 3\psi_1 = 0, \implies \psi_1 = \sqrt{\zeta} \tag{S39}$$

Finally, making a substitution $\psi_1 = e^{\frac{\zeta^2}{2a}(\varepsilon-\mu)}\sqrt{\zeta}\psi(\zeta)$ we obtain a much simpler differential equation (33) in the main body.

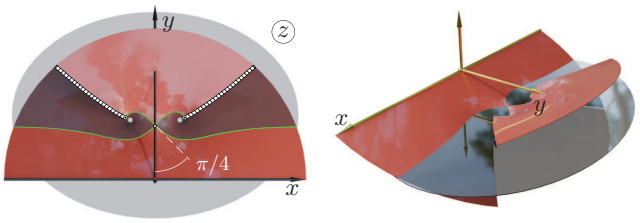

Figure S3: Exact anti-Stokes lines for the deformation profile $\varphi(z) = (z^2+1)^{-1}$ presented as a cross-section of the integral $h(z) = \mathrm{Im}\int_0^z \pi(t)\,dt$ and the level plane $h = h(z_+)$ (glass surface). (a) The top view. The anti-Stokes line marked as a green lines. We see that only lower anti-Stokes lines sprawl to $\pm\infty$ and become eventually parallel to the real axis. Upper anti-Stokes lines end at branch cuts origination from singular points $\varepsilon^2(z) = -1$. (b) Axonometric view of the cross section of the surface with a level glass plane.

C.2 Semiclassics for the potential with a pole

The equation for anti-Stokes lines is easily obtained in the vicinity of point z_p along the lines outlined in Section 35 (see Eq. S17). With the help of potential expansion (17) we obtain:

$$\begin{aligned} \mathrm{Im}\int_0^\zeta \pi(t)\,dt = \mathrm{Im}\left[-\frac{i\varepsilon}{a}\int_0^\zeta t dt\right] = 0 \;\Rightarrow \\ \arg\zeta = \frac{\arg a}{2} + \frac{\pi}{4} + \frac{\pi n}{2}, \quad n \in \mathbb{Z}. \end{aligned} \tag{S40}$$

Here, as before $\zeta \equiv z - z_p$. We see that anti-Stokes lines form $\pi/4$ directions (up to the rotation by $\arg a$) with the real axis. As an example we draw the portrait of the lines for a Lorentzian type profile $\varphi(z) = (z^2+1)^{-1}$ in Fig. S3.

C.3 Asymptotics of the erf function

The $\mathrm{erf}\,(z)$ function has the Stokes line on the imaginary axis. That means, its asymptotic changes as the argument of z crosses $-\pi/2$ direction. Starting from the very definition of the erf function one easily derives the following asymptotics in the neightborhood of directions $-\pi/4$ and $-3\pi/4$:

$$\begin{aligned} \mathrm{erf}(\zeta)\Big|_{\zeta=|\zeta|e^{-i\pi/4}} &= 1 - \frac{1}{\sqrt{\pi}}\frac{e^{-\zeta^2}}{\zeta} \\ \mathrm{erf}(\zeta)\Big|_{\zeta=|\zeta|e^{-3i\pi/4}} &= -1 - \frac{1}{\sqrt{\pi}}\frac{e^{-\zeta^2}}{\zeta} \end{aligned} \tag{S41}$$

Plugging in these asymptotics in to exact solution (34) we immediately obtain relations (35) and (36) in the main body.

D Semiclassical functions in the vicinity of the turning point z_p

First, it is logical to compute the main exponential factors (10), $S_\pm = \int_0^\zeta q_\pm(t)\,dt$. Here, the surprise awaits us, due to the subtlety of the work with a regular branch of momentum p entering the definition of $q_\pm$.

To understand the behavior of p, we need to track the behavior of function $\varphi^2(z)$. It has the second order pole at $z = z_p$:

$$\varphi^2(z) = -\frac{a^2}{(z-z_p)^2}, \quad z \to z_p. \tag{S42}$$

Looking at (S42), we see that there are two lines originating at the pole, along which $\varphi^2(z)$ stays negative and real. Those are the lines with directions $\arg a$ and $\arg a + \pi$ going to the right and left respectively (for concreteness, we assume that $|\arg a| < \pi/2$):

$$\zeta_{\text{right}} = |\zeta|\frac{a}{|a|} \qquad \zeta_{\text{left}} = -|\zeta|\frac{a}{|a|}, \tag{S43}$$

$$\varphi(\zeta_{\text{right}}) = i|\varphi(\zeta_{\text{right}})| \quad \varphi(\zeta_{\text{left}}) = -i|\varphi(\zeta_{\text{left}})| \tag{S44}$$

By the very definition of these lines they are the steepest ascent paths of function $\operatorname{Re}\varphi^2$. $\operatorname{Re}\varphi^2(z)$ changes from $-\infty$ to 0 as $\operatorname{Re} z \to \pm\infty$. To make things more transparent, we draw these lines for the Lorentzian function $\varphi(z) = (z^2+1)^{-1}$ in Fig. S4 (They flow below both branch cuts starting at $z_\pm$).

As point z moves from the pole z_p to the right along the steepest ascent line, it inevitably hits the branch point of p, z_+, which should be then circumvented from below. The same happens as the point moves to the left (point z_- is hit). The importance of these lines, therefore, rest in the fact that squared momentum p^2 stays real and positive to the right of z_+ and negative to the left (and vice versa for z_-). Therefore, the regular branch of p changes its sign as x moves from $+\infty$ to $-\infty$.

The definition of the regular branch of p, presented right after Eq. 11 in the main body, dictates its value once point z_+ is passed from right to left along the lower semicircle:

$$p(\zeta_{\text{right}}) = -i|p| \equiv e^{-i\pi/2}\sqrt{\varepsilon^2|\varphi^2| - \varepsilon^2 + \mu^2} \tag{S45}$$

Now we Taylor-expand the last equation in the vicinity of z_p while sticking to the right steepest ascent line:

$$p(\zeta_{\text{right}}) = e^{-i\pi/2}\left(\varepsilon|\varphi| - \frac{\varepsilon^2-\mu^2}{2\varepsilon|\varphi|}\right) + \ldots \tag{S46}$$

$$q_+(\zeta_{\text{right}}) = e^{i\pi/2}\frac{\varepsilon+\mu}{|\varphi|} \tag{S47}$$

Using (S47) we are ready to compute the main exponential factor S_+:

$$S_+(\zeta_{\text{right}}) = e^{i\pi/2}\int_0^{\zeta_{\text{right}}} \frac{\varepsilon+\mu}{|\varphi|}d\zeta_{\text{right}}, \tag{S48}$$

where the integration is assumed to be done along the right steepest ascent line. Next, we change according to (S43):

$$|\varphi| = \frac{|a|}{|\zeta|} = \frac{a}{\zeta_{\text{right}}} \to \frac{a}{\zeta}. \tag{S49}$$

The last equality in (S49) is the analytical continuation from the right steepest ascent line to its neighborhood. We obtain:

$$S_{+,>} = i\int_0^\zeta \zeta\frac{\varepsilon+\mu}{a}d\zeta = i(\varepsilon+\mu)\frac{\zeta^2}{2}. \tag{S50}$$

Now we need to compute pre-exponential factors $\xi_{1,\pm}$ (Eq. 12). In fact, we are *almost* ready to extract the correct regular branch of the square root $\xi_{1,+}$.

Surprisingly, function $p + \varphi\varepsilon$ entering the nominator of the expression under the square root of $\xi_{1,+}$ never vanishes in the complex plane. We assume its argument to be zero at $x \to +\infty$. One easily convinces oneself that as we arrive in the neighborhood of z_p along the right steepest ascent line, the argument of $p+\varphi\varepsilon$ becomes $\pi/2$. This is also clearly seen from eq. S46:

$$\varepsilon\varphi + p\Big|_{\text{right}} = e^{i\pi/2}\frac{\varepsilon^2-\mu^2}{2\varepsilon|\varphi|} \tag{S51}$$

Collecting (S46), (S47) and (S51) we obtain for $\xi_{1,+}$:

$$\xi_{1,+}\Big|_{\text{right}} = e^{3\pi i/4}\frac{\varepsilon+\mu}{\varepsilon}\sqrt{\frac{\varepsilon-\mu}{2|\varphi|^3}} + \ldots \tag{S52}$$

Making, as before, the analytical continuation $\zeta_{\text{right}} = \zeta$ we obtain:

$$\xi_{1+,>} = e^{3\pi i/4}\frac{\varepsilon+\mu}{\varepsilon}\sqrt{\frac{\varepsilon-\mu}{2}}\left(\frac{a}{\zeta}\right)^{3/2} \tag{S53}$$

Collecting (S53) and (S50) we obtain relation for $\psi_{1+,>}$ in (32) in the main body.

In the same manner we obtain relation for S_- and the rest of ξ_1:

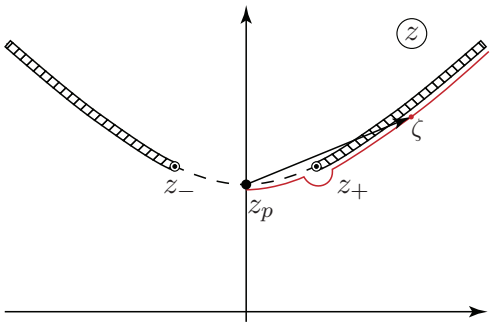

Figure S4: The curves $\operatorname{Im}\varphi^2(z) = 0$ for the Lorentzian function $\varphi(z) = (z^2+1)^{-1}$. The curves form hyperbola $y = \sqrt{x^2+1}$.

$$\begin{aligned}
\xi_{1+,<}(x) &= e^{-3\pi i/4}\frac{\varepsilon+\mu}{\varepsilon}\left[\frac{\varepsilon-\mu}{2}\right]^{1/2}\frac{1}{|\varphi|^{3/2}},\\
\xi_{1-,\gtrless}(x) &= e^{\pm i\pi/4}\left[\frac{2(\varepsilon-\mu)}{|\varphi|}\right]^{1/2}
\end{aligned} \tag{S54}$$

Performing analytical continuation in (S54) we get the rest of the asymptotic formula (32).

E Hamiltonian transformation and Born scattering

E.1 Derivation of the unitary transform $\hat{U}(x)$.

In the absence of magnetic field Hamiltonian reads:

$$H = v_F \sigma_y \hat{p} + \frac{\sigma_z}{2}(\varphi\hat{p} + \hat{p}\varphi) \tag{S55}$$

We introduce the following unitary transformation: $\hat{U}(x) = \exp(i\theta(x)\sigma_x)$, where $\theta(x)$ is real for real x. The next step is to apply this transformation to H. The transformed Hamiltonian $\tilde{H} = \hat{U}^\dagger H \hat{U}$ can be expressed as

$$\tilde{H} = v_F(\hat{U}^\dagger\sigma_y\hat{U})(\hat{U}^\dagger\hat{p}\hat{U}) + \frac{1}{2}(\varphi\hat{U}^\dagger\hat{p}\hat{U} + \hat{U}^\dagger\hat{p}\hat{U}\varphi)(\hat{U}^\dagger\hat{\sigma}_z\hat{U}). \tag{S56}$$

Let us write down the transformations of the individual terms: $\hat{U}^\dagger\hat{p}\hat{U} = \hat{p} + \theta'\sigma_x$, $\hat{U}^\dagger\sigma_y\hat{U} = (\sigma_y\cos 2\theta + \sigma_z \sin 2\theta)$, $\hat{U}^\dagger\sigma_z\hat{U} = (\sigma_z\cos 2\theta - \sigma_y \sin 2\theta)$. One plugs in these expressions into (S56).

Our goal is to find such function $\theta(x)$ that the term proportional to σ_y in the transformed Hamiltonian vanishes. We immediately obtain two consistent equations:

$$\begin{gathered} \sin 2\theta - \varphi\cos 2\theta = 0 \\ \frac{1}{2}\frac{d}{dx}[\sin 2\theta - \varphi\cos 2\theta] = 0 \end{gathered} \tag{S57}$$

This way we recover identity (39) and Hamiltonian (40) as well as (44) in the main body of the paper.

E.2 Exact eigenfunctions of the unperturbed Hamiltonian

The eigenfunctions of Hamiltonian (40) are needed for further perturbative analysis and can be easily found. The corresponding equation reads:

$$-i\left[v(x)\psi'_{1,2}(x) + \frac{1}{2}\psi_{1,2}(x)v'(x)\right] = \pm\varepsilon\psi_{1,2}(x) \tag{S58}$$

The l.h.s can be simplified with integrating factor as follows:

$$-i\sqrt{v}\left[\sqrt{v}\psi'_{1,2} + \frac{v'}{2\sqrt{v}}\psi_{1,2}\right] = -i\sqrt{v}[\sqrt{v}\psi_{1,2}]' \tag{S59}$$

And we trivially obtain eigenfunctions (41) in the main body. The important property of the eigenfunctions is the correct completeness relation. We obtain:

$$\sum_\sigma \int_{-\infty}^{\infty} \underset{\sigma}{\psi_\varepsilon}(x)\underset{\sigma}{\psi_\varepsilon}^\dagger(x)\frac{d\varepsilon}{2\pi} = \mathbf{1}\delta(x - x') \tag{S60}$$

where $\sigma = \leftrightarrows$ and $\mathbf{1}$ is the 2D unit matrix. Therefore, the correct measure counting the quantum eigenstates is $d\varepsilon/(2\pi)$. Also, of note, the normalization condition imposed on eigenfunctions. We need to make sure that condition

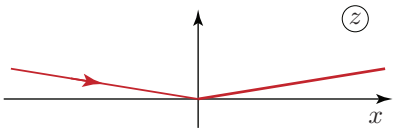

Figure S5: Deformation of the contour of the integral (S61)

$$\int_{-\infty}^{\infty} \underset{\sigma}{\psi_\varepsilon}^\dagger(x)\underset{\sigma}{\psi_{\varepsilon'}}(x)\,dx = \int_{-\infty}^{\infty} e^{\pm i(\varepsilon-\varepsilon')\tau(x)}\frac{dx}{v(x)} \propto \delta(\varepsilon - \varepsilon') \tag{S61}$$

is satisfied. Making a change $x \to \tau(x)$ we arrive at the integral

$$\int_{-\infty}^{\infty} e^{\pm i(\varepsilon-\varepsilon')\tau} d\tau = 2\pi\delta(\varepsilon - \varepsilon') \tag{S62}$$

Strictly speaking at $\varepsilon \neq \varepsilon'$, the integral (S61) converges only in the case when the contour is bent upward (or downward depending on the sign of coefficient in front of $\tau(x)$ in the exponent) in the complex plane, as shown in Fig. S5.

E.3 The Green's function

To build the perturbation theory we need a system's Green's function. We define the retarded Green's function as inverse Schrodinger operator, $\hat{G} = (\epsilon - \hat{H} + i0)^{-1}$. In the basis of the eigenfunctions it is expressed as

$$G(\epsilon; x, x') = \sum_\alpha \frac{\psi_\alpha(x)\psi_\alpha^\dagger(x')}{\epsilon - \varepsilon_\alpha + i0} \tag{S63}$$

Substituting eigenfunctions (41) and using the resolution of unity (S60), we get

$$G(\varepsilon; x, x') = \int \frac{d\varepsilon'}{2\pi}\frac{\varepsilon + \varepsilon'\sigma_z}{\sqrt{v(x)v(x')}}\frac{e^{i\varepsilon'(\tau(x)-\tau(x'))}}{(\varepsilon + i0)^2 - \varepsilon'^2} \tag{S64}$$

Integrating the last expression with the help of residue theorem we obtain the Green's function (43) in the main text.

F Steepest descent analysis of the Born approximation

F.1 The summary of our observations.

For exposition's clarity, we start with addressing the case of a single branch point z_0 (in the upper complex halfplane). The branch cut should be drawn in the upward direction $\mathrm{Re}[\varphi(z)^2] \to -\infty$. (See Fig. S6(a)). There is always the steepest descent path starting at the real axis and ending at branch point z_0. There are also two steepest descent paths to the left and to the right, stretching all the way to $+i\infty$. The simplified deformation of the contour spans two Riemann sheets of function $\tau(z)$ and is presented in Fig. S6(d). Despite the fact that this placement leads to the correct asymptotic of

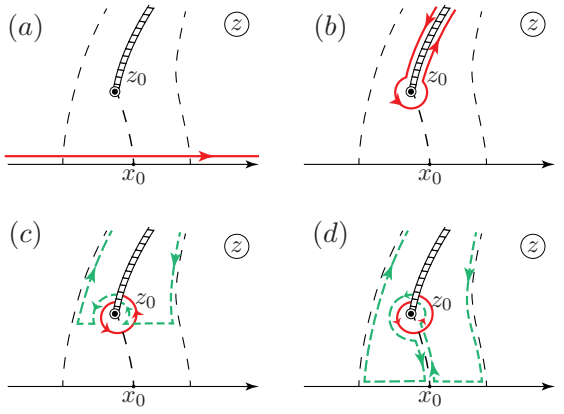

Figure S6: (a-d) The steepest descent paths (black dashed lines) and the deformation of the contour along the steepest descent paths of function $\mathrm{Re}\, i\tau(z)$. Color code of the contour means its placement on a different Riemann sheet of $\tau(z)$.

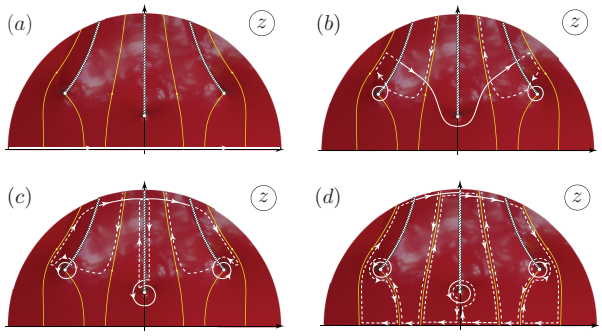

Figure S7: (a-d) The deformation of the contour for the function $\tau(z)$ for the profile deformation $\varphi(z) = ze^{-z^2/2}$. The final placement of the contour (d) corresponds to circumventing each branch point twice.

the integral (46) it is slightly inaccurate. It contains two horizontal segments on the real axis, which corresponds to the level lines of $\mathrm{Re}\,[i\tau(z)]$ rather than its steepest descent lines (i.e. the lines of maximal oscillation of $\exp[2i\varepsilon\tau(z)]$). Fortunately, these segments are positioned on the Riemann sheets of function $\tau(z)$ with smaller values of $\mathrm{Re}\, i\tau(z)$ leading to an exponentially small correction to the estimate of the integral (46).

What we discussed so far was the unrealistic case of the of $\tau(z)$ having a single branch point. Simple arguments (Appendix F.2) show that $\tau(z)$ always has an infinite number of branch points. Therefore, the deformation of the contour for a typical $\tau(z)$ is presented in Fig. S7. The principal contribution comes from the closest to the real axis branch point. Only three branch points happen to be inside the captured area of the Riemann surface of $\tau(z)$ in Fig. S7. However, we hope the reader grasps the general idea of the contour deformation from the illustration.

As we see from Fig. S7 the integral along the steepest descent contours sprawling from the branch points cancel each other. The contributions from other steepest descent lines are exponentially suppressed, since they

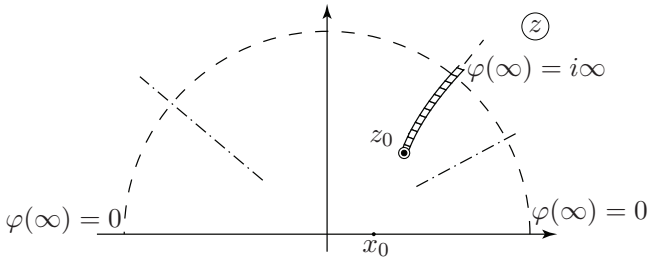

Figure S8: The schematic behavior of the potential function $\varphi(z)$ and $\tau(z)$. The dashed radian lines denote the boundaries of the change of the limit of $\varphi(\infty)$.

are positioned on the lower Riemann sheets.

F.2 The analytical properties of $\tau(z)$

We are going to argue that in general situation, there is a stationary $\mathrm{Re}\,\tau(z) = \mathrm{const}$ path connecting the real axis and the branch point z_0 of function $\tau(z)$.

Before proceeding further, let us make the following comment. The stationary path of a function of complex variable stemming from a particular point has 3 possible placements: i) it forms a closed contour returning to the starting point. ii) it ends in the singularity of the function (a pole, an essential singularity) iii) it has a corner at a branch point or at the stationary point. In particular, it turns by π and returns to the initial point in the case of the branch point of the second order (square root).

The behavior of function $\varphi(z)$ at $z \to \infty$. Since $\varphi(\pm\infty) = 0$ the function $\varphi(z)$ can't have a polynomial behavior at $z \to \infty$. Therefore, its Laurent series in the vicinity of ∞ has infinite amount of terms with positive powers of z and $z = \infty$ is an essential singularity.

According to Casorati-Weierstrass theorem, function $\varphi(z)$ can have any limiting value depending on the direction at which $z \to \infty$. We understand that due to the continuity of $\varphi(z)$, there is a sector (denoted by dash-dotted lines in Fig. S8) where $\varphi(\infty) = 0$. On the other hand, we may always find the direction $\arg z > 0$, $|z| \to \infty$ such that directional limit of $\varphi(|z|e^{i\arg z}) \to i\infty$ (dotted line in Fig. S8).

On the placement of the branch cut. Next, let us draw a branch cut of function $\tau(z)$ stemming from point z_0 upwards (away from the real axis) in the direction, where $\mathrm{Im}\,\varphi^2(z) = 0$. It is the steepest descent direction of $\mathrm{Re}\,\varphi^2(z)$ and precisely the direction of the dashed line in Fig. S8 discussed before. Therefore, $\varphi^2(z) + 1$ is real and negative and the square root $\sqrt{\varphi^2(z) + 1}$ is purely imaginary. That entails, in particular, that on both sides of the branch cut:

$$\tau(\infty \pm \delta) = \tau(z_0) \pm \frac{1}{i} \int_{z_0}^{\infty \pm \delta} \frac{dx + idy}{\sqrt{|\varphi^2(z) - 1|}}. \qquad \text{(S65)}$$

where $\infty \pm \delta$ denotes the points just below (above) the branch cut. It is important to note that the direction

of the branch cut is chosen in such a way that $\varphi^2(z) \to \infty$. Therefore, the branch cut at $z \to \infty$ lies above the limiting separatrix (see Fig. S8). Reading formula (S65) we point out that in the general situation

$$\frac{dy}{\sqrt{|\varphi^2(z)-1|}} \neq 0. \tag{S66}$$

The last expression then entails:

$$\mathrm{Re}\,\tau(\infty \pm \delta) \neq \mathrm{Re}\,\tau(z_0) \tag{S67}$$

It is also important to note that the integral entering (S65) can in principle be convergent.

The stationary path $\mathrm{Re}\,\tau(z) = \mathrm{Re}\,\tau(z_0)$**.** We notice that the real axis is the stationary path for $\mathrm{Im}\,\tau$: $\mathrm{Im}\,\tau = 0$. Therefore, all the stationary paths of $\mathrm{Re}\,\tau(z)$ stems vertically upwards and downwards from the real axis. One immediately convinces oneself that the upward direction is the steepest descent path for $\mathrm{Im}[\tau(z)]$. As was argued before, function $\varphi(z)$ ought to have an essential singularity at infinity, therefore, function $\tau(z)$ also has an essential singularity at $z \to \infty$. Since $\varphi(z)$ has no poles, function $\tau(z)$ has no stationary points.

That means, the stationary paths of $\mathrm{Re}\,\tau(z)$ stemming upwards from the real axis have only two options: they go to infinity, or they end at the second order branch point z_0 (and return back) to the starting point on the real axis.

Now we are going to argue that there always exists a point on a real axis with the value of $\tau(x)$ equal to the real part of $\tau(z_0)$ at the branch point. Indeed, the real semi line is the line of the steepest ascent of function $\tau(z)$ (In fact, $\tau(\pm\infty) = \pm\infty$). Therefore, it contains all possible values $\mathrm{Re}[\tau(z)]$ may assume in the complex plane. Consequently, there is a point x_0 on the real axis where $\tau(x_0) = \mathrm{Re}[\tau(z_0)]$. On the other hand, if the steepest descent curve stemming from x_0 doesn't enter z_0, it should go to infinity. The latter means that points with identical values of $\mathrm{Re}\,\tau(\infty) = \mathrm{Re}\,\tau(z_0)$. However, this is not possible, due to relation (S67). This way, we argued that there is always the steepest descent path stemming from some point x_0 on the real axis and ending at point z_0.

Other stationary paths. As was pointed out in the previous paragraph, function $\tau(z)$ has different limits at $z = \infty$ below and above branch cut: $\mathrm{Re}\tau_{\infty\downarrow}$, $\mathrm{Re}\tau_{\infty\uparrow}$. Finding the points on the real axis with the same values of τ (the latter are real) we can draw the steepest descent lines, as shown in Fig. S6.

G Semiclassical functions near the branch point p at $\mu \ll \varepsilon$

We start from the computation of q_+. Plugging in expansion (48) into expression (12) and retaining the two

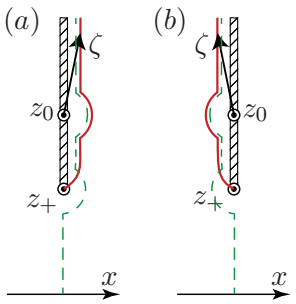

Figure S9: The integration contours (red curves) along the (a) right anti-Stokes line, (b) left anti-Stokes line. The green dashed lines represents the path along which the argument of p follows as point ζ travels from the real axis, where p is real and positive, upward along the right(a) and left (b) anti-Stokes lines

leading terms we have:

$$q_\pm(\zeta) = \frac{-\mu i + \varepsilon\sqrt{\frac{2i\zeta}{a}}}{\frac{2i\zeta}{a}} + ... \tag{S68}$$

Next, we integrate in the direction $\zeta = iy$ from the point z_+ along the right bank of the branch cut starting at point z_+ (the right anti-Stokes line, see Fig. S9(a)). The relative (with respect to z_0) coordinate of z_+ is found via the Taylor expansion:

$$\varphi(z) = i + \frac{\zeta}{a} + ... = i\sqrt{1 - \frac{\mu^2}{\varepsilon^2}} = i - \frac{i\mu^2}{2\varepsilon^2} + ...$$
$$\Rightarrow \zeta \equiv \zeta_+ = -\frac{ia}{2}\frac{\mu^2}{\varepsilon^2} + ... \tag{S69}$$

Now it is time to compute the regular branch of the square root (which is nothing but momentum $p = \varepsilon\sqrt{2i\zeta/a}$) entering q_+ in (S68). As seen from Fig. S9(a) (green dashed line), the argument of p rotates by π as ζ travels from real axis to the right anti-Stokes line. Therefore, $p = i|p|$ and the square root in (S68) is expended as: $\sqrt{2i\zeta/a} \equiv \sqrt{-2y/a} = i\sqrt{2y/a}$. Consequently, the semiclassical action reads:

$$S_+ = -\frac{\mu a}{2}\int_{\zeta_+}^{iy}\frac{d\zeta}{\zeta} + \varepsilon\int_0^y \sqrt{\frac{a}{2y}}\,dy \tag{S70}$$

where we changed the lower integration limit in the second integral from $y = -i\zeta_+$ to zero, since the upper integration limit obeys the condition $|y| \gg |\zeta_+|$ according to (52). This approximation, however, cannot be done with the first integral, since it becomes log divergent at $\zeta \to 0$. The first integral in (S70) is logarithmic, and we need to track correctly the change of the argument of ζ. It is easily red from Fig. S9(a): $\Delta\mathrm{arg}\zeta = \pi$. Finally, we obtain

$$S_+ = -\frac{\mu a}{2}\ln\frac{2y\varepsilon^2}{a\mu^2} - \frac{i\pi\mu a}{2} + \varepsilon\sqrt{2ay} \tag{S71}$$

Now we are ready to tackle the pre-exponential factors $\xi_{1,\pm}$ in (12). It is understood that $|\varphi\varepsilon/p| \sim \sqrt{|a\zeta|} \gg 1$.

Therefore, one can discard 1 under the square root in the definition of $q_\pm$. We already argued above in this section that the argument of p is $\pi/2$. The same is true for $\varphi = i$ in the vicinity of z_0. As a result $\arg[\varepsilon\varphi/p] = 0$. On the other hand we can discard term with μ in the zeroth order approximation in (S68). Therefore, $\arg q_+ = \arg p - \arg(\varphi^2 + 1) = \pi/2 - \pi = -\pi/2$. Finally, we have

$$\xi_{1,+} = |\xi_{1,+}|e^{-\frac{i\pi}{2}} = \frac{\varepsilon a}{y}e^{-\frac{i\pi}{2}}. \tag{S72}$$

Combining (S72), (S71) and plugging them into semiclassical wave function (12) we obtain $\psi_{+,>}$ (Eq. 54) in the main part of the paper. In complete analogy, one obtains relations (55) as well.

H Exact solution near the branch point p at $\mu \ll \varepsilon$

To solve (56) we use the Laplace method of solution of differential equation with linear coefficients outlined in Appendix B. Polynomials P and Q are red from equation (56):

$$P = (3i - 2a\mu)t + \varepsilon^2 a, \quad Q = 2it^2. \tag{S73}$$

Performing integration $\int (P/Q)\,dt$ and changing $t = \varepsilon s$ we obtain the solution in the form (57) (up to a contant in front of the integral). Function $V(\zeta, t)$ from (S22) becomes:

$$V(\zeta, s) = \exp\left(\zeta\varepsilon s + \frac{\varepsilon a i}{2s}\right) s^{ia\mu + \frac{3}{2}}. \tag{S74}$$

To define the regular branches of the multivalued function $s^{ia\mu}$ entering the exact solution and function V, a branch cut should be drawn from the point $s = 0$. The most suitable direction is upward.

H.1 The placement of the contour

We are looking for points in the complex plane s where function $V(\zeta, s)$ assumes identical values. The points which are the easiest to identify are the ones where V vanishes.

Suppose ζ is initially placed on the right anti-Stokes line (Fig. 5(a) right). As in the main body, let us assume without loss of generality a to be real. We see that if $s \to +i\infty$ function $V(\zeta, s) \to 0$. On the other hand, if $s \to 0$ in vertical direction (see Fig 5(a) left) V vanishes as well. Therefore, contour C depicted in Fig. 5(a) satisfies the principal condition of the placement.

H.2 Saddle point approximation, right anti-Stokes line

To match the exact solution with semiclassical expressions, we need to find the asymptotics of (57) at large ζ. As pointed out in the main body of the paper, the exponent function (58) has two saddles $s_{1,2}$, the right being the one giving the correct semiclassical exponential (54). The steepest descent directions at the saddles are given by Eq. S31 and read:

$$\alpha(s_{1,2}) = \pm\frac{\pi}{4} + \pi n, \; n \in \mathbb{Z} \tag{S75}$$

Computing the integral in the saddle point approximation and taking into account that the steepest descent direction at s_1 is $\pi/4$ and comparing the result with (54) we are able to fixate the constant in front of the integral in (57).

H.3 Saddle point approximation, left anti-Stokes line

Now we need to build an analytical continuation of the exact solution given by integral (57) once ζ goes from the right to the left anti-Stokes line and rotates by 2π in the clockwise direction.

Contour C should guarantee the vanishing of $V(\zeta, s)$ at $s \to \infty$ during all the transformation of ζ. To compensate for the change of argument of ζ by -2π, the end point of the contour should rotate by 2π in the complex plane of s (as depicted in Fig. 5(c)) turning it into a spiral. Since the branch cut obstructs the rotation of the contour, the latter should cross the branch cut and continue on the second Riemann sheet of multivalued function $s^{ia\mu - 1/2}$. All the arguments of s on the second Riemann sheet are related to the ones on the first one by 2π rotation: $s|_{\text{second}} = s|_{\text{first}} e^{2\pi i}$.

The steepest descent paths of function f (58) are the same on both Riemann sheets. Therefore, to find the asymptotics of the integral after the transformation $\zeta \to \zeta e^{2\pi i}$, the contour is deformed along the steepest descent curves on both Riemann sheets, as shown in Fig. 6. The arc of the contour at ∞ (Fig. 6(a)) does not contribute to the integral, since the integrand vanishes at all points of the arc.

From the structure of the contour in Fig. (6) we see that both saddles now contribute to the integral. Saddle s_2 is passed in $-\pi/4$ direction, while saddle s_1 is passed twice. The contribution of the saddle from the second Riemann sheet is identical to the one from the first Riemann sheet up to a constant factor coming from the different value of the multivalued function at saddle s_1:

$$s_1^{i\mu a - 1/2} \to s_1^{i\mu a - 1/2} e^{2\pi i(i\mu a - 1/2)}. \tag{S76}$$

The last equation leads directly to (60) after simple algebra.

References

[1] L. D. Landau and E. M. Lifshitz, *Quantum mechanics: non-relativistic theory*, vol. 3 (Elsevier, 2013).

[2] E. Goursat, *A Course in Mathematical Analysis: pt. 2. Differential equations.* [c1917, vol. 2 (Dover Publications, 1916).